ISSN 1674-1056
http://cpb.iphy.ac.cn
http://iopscience.iop.org/cpb
中国物理 B
Chinese Physics
中国物理 Chinese Physics B

Physical properties of B_4N_4-I and B_4N_4-II: First-principles study

Zhenyang Ma(马振洋), Peng Wang(王鹏), Fang Yan(阎芳), Chunlei Shi(史春蕾), Yi Tian(田毅)

Citation: Chin. Phys. B . 2019, 28(3): 036101. **doi:** 10.1088/1674-1056/28/3/036101
Journal homepage: http://cpb.iphy.ac.cn; http://iopscience.iop.org/cpb

What follows is a list of articles you may be interested in

Mechanical, elastic, anisotropy, and electronic properties of monoclinic phase of *m*-$Si_xGe_{3-x}N_4$

Zhen-Yang Ma(马振洋), Fang Yan(阎芳), Su-Xin Wang(王苏鑫), Qiong-Qiong Jia(贾琼琼), Xin-Hai Yu(于新海), Chun-Lei Shi(史春蕾)

Chin. Phys. B . 2017, 26(12): 126105. **doi:** 10.1088/1674-1056/26/12/126105

Electronic, optical, and mechanical properties of BN, AlN, and InN with zinc-blende structure under pressure

A R Degheidy, E B Elkenany

Chin. Phys. B . 2017, 26(8): 086103. **doi:** 10.1088/1674-1056/26/8/086103

Theoretical prediction of new C-Si alloys in *C*2/*m*-20 structure

Xiangyang Xu(徐向阳), Changchun Chai(柴常春), Qingyang Fan(樊庆扬), Yintang Yang(杨银堂)

Chin. Phys. B . 2017, 26(4): 046101. **doi:** 10.1088/1674-1056/26/4/046101

Role of helium in the sliding and mechanical properties of a vanadium grain boundary：A first-principles study

Zhou Hong-Bo, Jin Shuo, Zhang Ying, Shu Xiao-Lin, Niu Liang-Liang

Chin. Phys. B . 2014, 23(5): 056104. **doi:** 10.1088/1674-1056/23/5/056104

Effects of chromium on structure and mechanical properties of vanadium：A first-principles study

Gui Li-Jiang, Liu Yue-Lin, Wang Wei-Tian, Zhang Ying, Lü Guang-Hong, Yao Jun-En

Chin. Phys. B . 2013, 22(10): 106109. **doi:** 10.1088/1674-1056/22/10/106109

Physical properties of B_4N_4-I and B_4N_4-II: First-principles study*

Zhenyang Ma(马振洋), Peng Wang(王鹏)†, Fang Yan(阎芳),
Chunlei Shi(史春蕾), and Yi Tian(田毅)

Key Laboratory of Civil Aircraft Airworthiness Technology, Civil Aircraft Airworthiness and Repair Key Laboratory of Tianjin, School of Airworthiness, Civil Aviation University of China, Tianjin 300300, *China*

(Received 9 September 2018; revised manuscript received 20 December 2018; published online 23 January 2019)

The structural, mechanical, electronic, mechanical anisotropy, and thermal properties of boron nitride (BN) polymorphs, such as B_4N_4-I and B_4N_4-II, are investigated under ambient pressure utilizing first-principles generalized gradient approximation calculations using an ultrasoft pseudopotential scheme. The phonon spectra and elastic constants reveal that B_4N_4-I is dynamically and mechanically stable at the pressure of 0 GPa and temperature of 0 K. Anisotropic calculations indicate that both B_4N_4-I and B_4N_4-II exhibit higher anisotropy of Young's modulus than cubic BN (c-BN). B_4N_4-II and B_4N_4-I present indirect and wide band gaps of 5.32 eV and 4.86 eV, respectively. In addition, B_4N_4-I is more brittle than B_4N_4-II. Moreover, the minimum thermal conductivity, κ_{min}, of B_4N_4-II at 300 K is 1.92 W/(cm·K), which is slightly higher than those of B_4N_4-I and c-BN (1.84 W/(cm·K) and 1.83 W/(cm·K), respectively. However, κ_{min} of B_4N_4-I is slightly higher than that of c-BN.

Keywords: BN polymorphs, mechanical properties, electronic properties, mechanical anisotropic properties

PACS: 61.50.–f, 61.50.Ah, 71.20.Nr, 71.55.Cn **DOI:** 10.1088/1674-1056/28/3/036101

1. Introduction

Since cubic boron nitride (c-BN) was discovered in 1957,[1] BN polymorphs[2–10] and other superhard materials that consist of light elements, such as C–N,[11–17] B–C–O,[18–22] and B–C–N compounds,[23–26] have been investigated. The bulk moduli (B) or hardness (H) values of many compounds are higher than those of c-BN. For example, the B of P-BN that was calculated using the local-density approximation (LDA) method was 403 GPa,[8] which was slightly higher than that of c-BN (397 GPa) calculated using the same method.[6] The bulk (B) and shear (G) moduli (400 GPa and 424 GPa, respectively) of *Imm*2-BCN[25] calculated using LDA were both higher than those of c-BN (407 GPa). Moreover, the B of $P3m1$-BCN[26] calculated using the LDA and generalized gradient approximation (GGA) methods were both slightly higher than the corresponding values of c-BN calculated using the same methods.

Ma *et al.*[2] proposed an orthorhombic symmetry with the *Pnma* space group for BN. The structure of *Pnma*-BN consists of four N and four B atoms buckled in a conventional cell through sp^3-hybridized bonds. Furthermore, Ma *et al.*[2] determined that *Pnma*-BN is an insulator with an indirect band gap of 7.18 eV, and is brittle at ambient pressure. Hromadová and Martoňák[3] investigated the structural transitions of BN in the 300–3000 K temperature range and 20–31 GPa pressure range. Fan *et al.*[6] investigated an orthorhombic phase, *Pbca*-BN, using first-principle calculations, and determined that the H of *Pbca*-BN was 60.1 GPa. Therefore, *Pbca*-BN could be a potential superhard material. Based on a global structural search and first-principles calculations, Dai *et al.*[9] predicted two types of porous BN polymorphs, and their networks could be established with zigzag BN nanoribbons, denoted as dz2-BN and dz4-BN (space groups *Ima*2 and *Ama*2, respectively). These structures were determined to be mechanically and dynamically stable as well as thermally stable at 1000 K. The surface areas of dz2-BN and dz4-BN were large, and it has been revealed that both dz2-BN and dz4-BN exhibit hydrogen storage properties. Furthermore, dz4-BN was established to be a direct band gap semiconductor material, and also exhibited properties suited for optoelectronic and photonic applications.

Li *et al.*[7] analyzed the structure and properties of primitive-centered tetragonal BN (pct-BN) and determined that pct-BN was more energetically favorable than hexagonal BN (h-BN) when the pressure P exceeded 8.8 GPa, and was still dynamically stable when P was lower than 120 GPa. The calculated H (51 GPa) indicated that pct-BN was also a potential superhard material. Kuzubov *et al.*[4] proposed a novel BN structure, hP3-BN, which consisted of sp^3-bonded atoms. The novel hP3-BN exhibited superhard and superdense properties, as well as a higher B than c-BN. In addition, Kuzubov *et al.*[4] also established that hP3-BN was an insulator. Recently, Germaneau *et al.*[5] applied first-principles simulations to investigate three proposed types of BN polymorphs: B_4N_4-I, B_4N_4-II, and B_4N_4-III. They determined the H of B_4N_4-I, B_4N_4-II (space group $P1$), and B_4N_4-III to be 46.5 GPa, 66.8 GPa, and 41.7 GPa, respectively, suggesting that these three types of BN

*Project supported by the National Natural Science Foundation of China (Grant No. 61601468), the Fundamental Research Funds for the Central Universities, China (Grant No. 3122014C024), and the Fund for Scholars of Civil Aviation of the University of China (Grant No. 2013QD06X).

†Corresponding author. E-mail: wangpengcauc@163.com

© 2019 Chinese Physical Society and IOP Publishing Ltd

polymorphs are all potential superhard materials. In addition, B_4N_4-I, B_4N_4-II, and B_4N_4-III were revealed to be dynamically and mechanically stable. While the structural, mechanical, and electronic properties of B_4N_4-I, B_4N_4-II, and B_4N_4-III have been previously investigated, the elastic anisotropy of B_4N_4-II has not been studied yet. We systemically investigated the structural, mechanical, mechanical anisotropy, and electronic properties, as well as the minimum thermal conductivity, κ_{min}, of B_4N_4-II and B_4N_4-I under pressure. The electronic properties of B_4N_4-II and B_4N_4-I were estimated using the HSE06 hybrid functional.[27] B_4N_4-II and B_4N_4-I presented indirect and wide band gaps of 5.32 eV and 4.86 eV, respectively. Moreover, the κ_{min} values of B_4N_4-II and B_4N_4-I (1.92 W/(cm·K) and 1.84 W/(cm·K), respectively, were both slightly higher than that of c-BN (1.83 W/(cm·K)).

2. Computational details and theory

We investigated the structural, mechanical, mechanical anisotropy, and electronic properties of B_4N_4-I and B_4N_4-II in detail by utilizing first-principles calculations based on density functional theory (DFT).[28] We predicted the physical properties of B_4N_4-I and B_4N_4-II using DFT based on the Cambridge serial total energy package (CASTEP) code[29] combined with the Vanderbilt ultrasoft pseudopotential.[30] The Broyden–Fletcher–Goldfarb–Shanno[31] minimization scheme was used for geometry optimizations. The maximum ionic displacement was within 5×10^{-4} Å, the maximum stress was within 0.02 GPa, the self-consistent convergence of the total energy was 5×10^{-6} eV/atom, and the maximum force on the atom was 0.01 eV/Å. The exchange and correlation were approximated using GGA parameterized by Perdew, Burkeand, and Ernzerrof (PBE)[32] and LDA, based on Ceperley–Alder data, as parameterized by Perdew and Zunger (CA-PZ).[33] The plane-wave basis was set for the prediction of the physical properties and structure calculations, and its energy cutoff was 500 eV. Proper k-point grids of 16 ×10× 8 and 14 ×4× 10 were used in the Brillouin zones for B_4N_4-I and B_4N_4-II, respectively, utilizing the Monkhorst–Pack method.[34]

3. Results and discussion

The crystal structures of B_4N_4-I and B_4N_4-II are illustrated in Figs. 1(a) and 1(b), respectively. Figures 1(c) and 1(d) depict the crystal structures of B_4N_4-I and B_4N_4-II along the [001] direction, respectively. The red and blue spheres represent B and N atoms, respectively. Both B_4N_4-II and B_4N_4-I consist of six-membered B and N rings, while the ten-membered rings in the structure of B_4N_4-I are normal to the [001] direction (see Fig. 1(c)). The lattice parameters and crystal densities of B_4N_4-II and B_4N_4-I, together with those of other BN polymorphs, are listed in Table 1. In the present study, the crystal structures of B_4N_4-II and B_4N_4-I were optimized using the PBE and CA-PZ functionals, and the calculation results are all listed in Table 1. As seen in Table 1, the GGA–PBE functional calculation results of c-BN are much closer to the corresponding experimental results.[25,35,36]

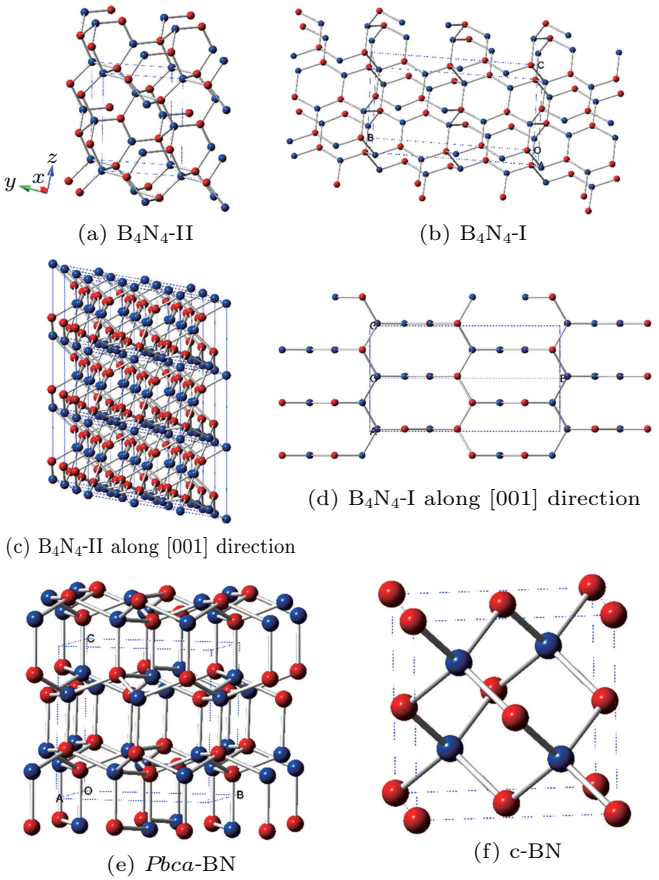


Fig. 1. Crystal structures of (a) B_4N_4-II, (b) B_4N_4-I, (c) B_4N_4-II along the [001] direction, (d) B_4N_4-I along the [001] direction, (e) *Pbca*-BN, and (f) c-BN.

Thus, the physical properties of B_4N_4-II and B_4N_4-I were used to determine their crystal structures from the optimized function of GGA–PBE. For *Pbca*-BN and *Pnma*-BN, the calculated lattice parameters were in agreement with the theoretical values. B_4N_4-I presented monoclinic symmetry and the *Cc* space group. The B and N atoms in B_4N_4-II both presented two inequivalent positions: the B atoms occupied the B1 $(-1.3796, -1.7475, -0.9918)$ and B2 $(-0.8858, -0.9986, -0.5003)$ positions, and the N atoms occupied the N1 $(-0.3723, -1.0042, -0.1710)$ and N2 $(-0.7512, -0.8586, -0.1513)$ positions in the conventional cell. In addition, B_4N_4-II and B_4N_4-I only contained sp^2 hybridized atoms. Twelve and six different bonds were identified in $P1$-B_4N_4-II and B_4N_4-I, respectively. The bond lengths of B_4N_4-II were 1.3768 Å, 1.4755 Å, 1.4805 Å, 1.4851 Å, 1.4960 Å, 1.5587 Å, 1.5753 Å, 1.5782 Å, 1.5795 Å, 1.5800 Å, 1.5834 Å, and 1.6073 Å, and the average bond length was 1.5313 Å. Meanwhile, the bond lengths of B_4N_4-I were 1.4372 Å, 1.4521 Å, 1.4538 Å, 1.4695 Å, 1.4701 Å,

and 1.4848 Å, and they were all shorter than those of c-BN (1.5653 Å). In addition, the polymorphs of the *Cc* phases of BN were named *Cc* B_4N_4-I[5] and *Cc* (ICSD# 162882).[37] Furthermore, the crystal structures of *Pbca*-BN and c-BN were compared, and the corresponding images are shown in Figs. 1(e) and 1(f), respectively. The calculated B–N bond distance of *Pbca*-BN was 1.5878 Å at ambient pressure,[6] the B–N bond lengths of *Pnma*-BN[2] were 1.6518 Å, 1.5098 Å, and 1.5554 Å, and the mean bond length was 1.5568 Å. The B–N bond lengths of B_4N_4-I and B_4N_4-II were 1.4565 Å and 1.5313 Å, respectively, which were both shorter than those of *Pbca*-BN, *Pnma*-BN, and c-BN. This was mainly attributed to the sp^2 and sp^3 hybridizations of the atoms of B_4N_4-I and B_4N_4-II, respectively.

Table 1. Lattice parameters and crystal densities of B_4N_4-I, B_4N_4-II, and other BN polymorphs.

Material	Method	*a*/Å	*b*/Å	*c*/Å	*β*/(°)	*ρ*/g·cm^{-3}
B_4N_4-II	GGA	2.622	4.043	4.935	81.81	3.323
	GGA[a]	2.609	4.025	4.921	81.85	3.274
B_4N_4-I	GGA	3.294	9.421	4.675	116.67	2.543
	LDA	3.121	9.379	4.591	115.44	2.716
	LDA[a]	3.129	9.470	4.616	115.16	2.662
Pnma-BN	GGA	4.890	2.589	4.284		3.040
	LDA	4.795	2.557	4.243		3.169
	LDA[b]	4.760	2.580	4.290		3.129
Pbca-BN	GGA	5.099	4.422	4.398		3.325
	GGA[c]	5.110	4.434	4.399		3.308
	LDA	5.041	4.379	4.332		3.448
	LDA[c]	5.046	4.380	4.339		3.438
c-BN	GGA	3.626				3.458
	LDA	3.569				3.626
	Exp.[d]	3.620				3.475

[a]Ref. [5], [b]Ref. [2], [c]Ref. [6], [d]Refs. [25], [35], [36].

Table 2. Elastic constants (in GPa) of B_4N_4-I, B_4N_4-II, and other BN polymorphs.

Materials	C_{11}	C_{12}	C_{13}	C_{15}	C_{22}	C_{23}	C_{25}	C_{33}	C_{35}	C_{44}	C_{46}	C_{55}	C_{66}
B_4N_4-II	565	129	21	49	763	152	–38	892	–29	371	–32	196	252
B_4N_4-I	204	148	171	123	716	158	35	483	183	124	71	174	166
Pnma-BN	392	99	256		770	116		675		299		272	187
Pbca-BN	769	145	133		870	105		716		307		255	340
	772[a]	135	139		885	92		716		312		257	357
c-BN	788	160						443					
	779[b]	165						446					

[a]Ref. [6], [b]Ref. [25].

The calculated elastic constants of B_4N_4-I and B_4N_4-II, together with those of other BN polymorphs *Pnma*-BN, c-BN, and *Pbca*-BN are illustrated in Table 2. B_4N_4-II belongs to the *P*1 space group, which presents the most independent elastic constants of 230 space groups. We only provide some of the main elastic constants for the *P*1 space group in Table 2. The remaining independent elastic constants of B_4N_4-II C_{14}, C_{16}, C_{24}, C_{26}, C_{34}, C_{36}, C_{45}, and C_{56} are 6 GPa, −65 GPa, −40 GPa, −162 GPa, −5 GPa, −18 GPa, −32 GPa, and 6 GPa, respectively. B_4N_4-I presents monoclinic symmetry. This includes only 13 independent elastic constants, and they meet the mechanical stability criteria. The mechanical stability criteria of monoclinic symmetry are given by the following formulas:[38,39]

$$
\begin{aligned}
&C_{ii} > 0 \quad (i = 1-6),\\
&C_{11}+C_{22}+C_{33}+2(C_{12}+C_{13}+C_{23}) > 0,\\
&C_{33}C_{55}-C_{35}^2 > 0, \quad C_{44}C_{66}-C_{46}^2 > 0,\\
&C_{22}+C_{33}-2C_{23} > 0,\\
&C_{22}(C_{33}C_{55}-C_{35}^2)+2C_{23}C_{25}C_{35}-C_{23}^2C_{55}-C_{25}^2C_{33} > 0,\\
&2[C_{15}C_{25}(C_{33}C_{12}-C_{13}C_{23})+C_{15}C_{35}(C_{22}C_{13}-C_{12}C_{23})\\
&+C_{25}C_{35}(C_{11}C_{23}-C_{12}C_{13})]-[C_{15}^2(C_{22}C_{33}-C_{23}^2)\\
&+C_{25}^2(C_{11}C_{33}\ -C_{13}^2)+C_{35}^2(C_{11}C_{22}-C_{12}^2)]\\
&+(C_{11}C_{22}C_{33}-C_{11}C_{23}^2-C_{22}C_{13}^2\\
&-C_{33}C_{12}^2+2C_{12}C_{13}C_{23})C_{55} > 0.
\end{aligned}
$$

The calculated results indicated that *Cc*-BN was mechanically stable.

The calculated elastic moduli of B_4N_4-I, B_4N_4-II, *Pbca*-BN, *Pnma*-BN, and c-BN are listed in Table 3. The elastic moduli (*B* and *G*) were estimated using the Voigt–Reuss–Hill approximation.[40] The B_V, B_R, G_R, and G_V values could be calculated using the following expressions:[38,41]

$$
\begin{aligned}
B_V &= [C_{11}+C_{22}+C_{33}+2(C_{12}+C_{13}+C_{23})]/9;\\
B_R &= \Omega(a+b+c+d+e+f)^{-1},
\end{aligned}
$$

$$
\begin{aligned}
\Omega &= 2[C_{15}C_{25}(C_{33}C_{12}-C_{13}C_{23})+C_{15}C_{35}(C_{22}C_{13}-C_{12}C_{23})\\
&\quad +C_{25}C_{35}(C_{11}C_{23}-C_{12}C_{13})]-[C_{15}^2(C_{22}C_{33}-C_{23}^2)\\
&\quad +C_{25}^2(C_{11}C_{33}-C_{13}^2)+C_{35}^2(C_{11}C_{22}-C_{12}^2)]\\
&\quad +C_{55}(C_{11}C_{22}C_{33}-C_{11}C_{23}^2-C_{22}C_{13}^2\\
&\quad -C_{33}C_{12}^2+2C_{12}C_{13}C_{23}),\\
a &= (C_{33}C_{55}-C_{35}^2)(C_{11}+C_{22}-2C_{12}),\\
b &= (C_{23}C_{55}-C_{25}C_{35})(2C_{12}-2C_{11}-C_{23}),\\
c &= (C_{13}C_{35}-C_{15}C_{33})(C_{15}-2C_{25}),\\
d &= (C_{13}C_{55}-C_{15}C_{35})(2C_{12}+2C_{23}-C_{13}-2C_{22}),\\
e &= (C_{13}C_{25}-C_{15}C_{23})(C_{25}-C_{15}),\\
f &= C_{11}(C_{22}C_{55}-C_{25}^2)-C_{12}(C_{12}C_{55}-C_{15}C_{25})\\
&\quad +C_{15}(C_{12}C_{25}-C_{15}C_{22})+C_{25}(C_{23}C_{35}-C_{25}C_{33});\\
G_{\rm V} &= [C_{11}+C_{22}+C_{33}+3(C_{44}+C_{55}+C_{66})\\
&\quad -(C_{12}+C_{13}+C_{23})]/15,\\
G_{\rm R} &= 15\left[4(f+h+i+j+k+l)/\Omega\right.\\
&\quad \left.+\left(3g/\Omega+\frac{C_{44}+C_{66}}{C_{44}+C_{66}-C_{46}^2}\right)\right]^{-1},\\
h &= (C_{33}C_{55}-C_{35}^2)(C_{11}+C_{22}+C_{12}),\\
i &= (C_{23}C_{55}-C_{25}C_{35})(C_{11}-C_{12}-C_{23}),\\
j &= (C_{13}C_{35}-C_{15}C_{33})(C_{15}+C_{25}),\\
k &= (C_{13}C_{55}-C_{15}C_{35})(C_{22}-C_{23}-C_{12}-C_{13}),\\
l &= (C_{13}C_{25}-C_{15}C_{23})(C_{15}-C_{25}),\\
g &= C_{11}C_{22}C_{33}-C_{11}C_{23}^2-C_{22}C_{13}^2\\
&\quad -C_{33}C_{12}^2+2C_{12}C_{13}C_{23}.
\end{aligned}
$$

From Table 3, one can determine that the B value of B_4N_4-II is slightly lower than that of *Pnma*-BN, while the G value of B_4N_4-II is higher than that of *Pnma*-BN. The G and B values of *Cc*-BN are the smallest among all these BN polymorphs. Furthermore, E and Poisson's ratio v can be estimated using the following equations: $E = 9BG/(3B+G)$ and $v = (3B-2G)/[2(3B+G)]$.[40,42,43] The E values of B_4N_4-II and B_4N_4-I are similar to the G and B values. In addition, the equation $H = 2(G^3/B^2)^{0.585} - 3$[44] was used to estimate the hardness of B_4N_4-II and B_4N_4-I. We calculated the H values of B_4N_4-II, B_4N_4-I, *Pnma*-BN, *Pbca*-BN, and c-BN using Chen's[44] and Lyakhov and Oganov's (L–O's) models.[45] The H values calculated using Chen's and L–O's models are also listed in Table 3. In addition, the H values of B_4N_4-I and B_4N_4-II were calculated using Gao's model.[46] Many differences can be observed between the H values calculated using Chen's and L–O's models. Similar results have also been reported by Xing *et al.*[47] and Bu *et al.*[48] The main reason for these differences was attributed to the empirical formulas either overestimating or underestimating the H values of the materials. According to Germaneau *et al.*,[5] the H value of B_4N_4-II was 66.821 GPa. Some studies[48–50] have demonstrated that Gao's model overestimated the hardness of extremely anisotropic compounds. According to Chen's model, the H of B_4N_4-I was 43.64 GPa, which suggested that B_4N_4-I was a potential superhard material.

Table 3. Calculated elastic moduli (the bulk (B), shear (G), and Young's (E) moduli, in GPa) and hardness (H in GPa) of B_4N_4-II, B_4N_4-I, *Pnma*-BN, *Pbca*-BN, and c-BN.

Material	B	G	B/G	E	v	$H_{\rm Chen}$	$H_{\rm Gao}$	$H_{\rm L-O}$
B_4N_4-II	294	266	1.11	613	0.152	17.65	66.82	38.68
B_4N_4-I	181	121	1.50	297	0.227	43.64	46.51	7.74
Pnma-BN	298	227	1.31	543	0.196	31.76	–	33.32
Pbca-BN	340	312	1.09	717	0.148	49.05	–	38.88
	344[a]	316	1.09	718	0.140	49.51	–	–
c-BN	369	386	0.96	859	0.112	65.72	–	50.38
	370[b]	384	0.96	856	0.120	64.88	–	–

[a]Ref. [6], [b]Ref. [25].

Hence, both the Pugh (B/G) ratio and v can define the quantitative index to assess the brittle or ductile behavior of crystal materials. A high B/G value (> 1.75) of a solid would indicate its ductile behavior, while a low B/G value (< 1.75) would usually indicate its brittle behavior.[51] Moreover, high v values (> 0.26) usually indicate ductile materials.[52] The values of v and B/G of B_4N_4-II, *Pnma*-BN, B_4N_4-I, *Pbca*-BN, and c-BN are listed in Table 3. The values of B/G and v for B_4N_4-II were 1.11 and 0.152 at the pressure of 0 GPa, and the corresponding values for B_4N_4-I were 1.50 and 0.227 at the pressure of 0 GPa, respectively. Among these BN polymorphs, c-BN was the most brittle and B_4N_4-I was the least brittle. The Debye temperature $\Theta_{\rm D}$ has been frequently used in semiempirical and phase diagrams studies. The Debye model provides a simple but very effective Gibbs energy method for describing the crystal phase of phonons.[2]

The $\Theta_{\rm D}$ and mean sound velocity $v_{\rm m}$ can be approximately estimated using the following relationships:[53,54]

$$
\begin{aligned}
&\Theta_{\rm D} = (h/k_{\rm B})[(3n/4\pi)(N_{\rm A}\rho/M)]^{1/3}v_{\rm m},\\
&v_{\rm m} = [(2/v_{\rm t}^3+1/v_{\rm l}^3)/3]^{-1/3},\\
&v_{\rm l} = [(B+4G/3)/\rho]^{1/2},\quad v_{\rm t} = (G/\rho)^{1/2},
\end{aligned}
$$

where h is Planck's constant, $k_{\rm B}$ is Boltzmann's constant, ρ is the crystal density, $N_{\rm A}$ is Avogadro's number, n is the num-

ber of atoms in the molecule, M is the molecular weight, v_t is the transverse sound velocity, and v_l is the longitudinal sound velocity. The crystal density of B_4N_4-II is the smallest of all these BN polymorphs, while the crystal density of B_4N_4-I is close to that of *Pbca*-BN and slightly lower than that of c-BN. The Θ_D values of B_4N_4-II and B_4N_4-I are 1601 K and 1131 K, respectively, which are both slightly lower than those of *Pbca*-BN (1734 K within the GGA–PBE level)[6] and wurtzite-BN (space group: $P6_3mc$, 1905 K).

We then investigated the mechanical anisotropy of G and E of B_4N_4-II and B_4N_4-I. The formulas for calculating G and E were reported by Fan *et al.*[26] and Marmier *et al.*,[55] respectively. The three-dimensional (3D) surface figures and the two-dimensional (2D) representations of G for B_4N_4-II and B_4N_4-I are plotted in Fig. 2. From Fig. 2, it can be observed that the G values of B_4N_4-II and B_4N_4-I exhibit varying degrees of elastic anisotropy. We used the ratio of the maximal and minimal values of E to quantify the magnitude of the elastic anisotropy of each BN polymorph analyzed in this study. The maximal and minimal values of G for B_4N_4-II, B_4N_4-I, and c-BN are listed in Table 4. From Table 4, it is obvious that

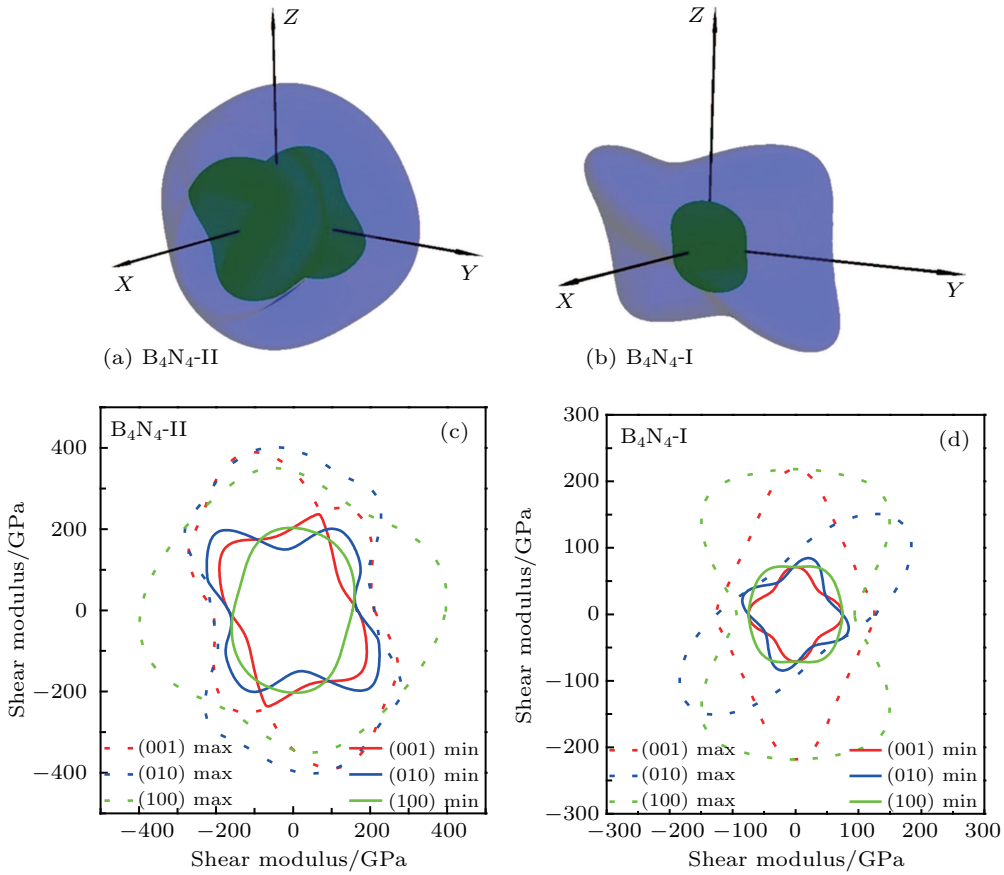


Fig. 2. Schematic 3D surface images of (a) B_4N_4-II and (b) B_4N_4-I; 2D representation of the shear modulus (G) of (c) B_4N_4-II and (d) B_4N_4-I. The purple and green curved surfaces in the 3D surface images of B_4N_4-II and B_4N_4-I represent the maximum and minimum values of G. The red, blue, and green lines in the 2D diagrams of G represent the (001), (010), and (100) planes, respectively. The dashed lines in panels (c) and (d) represent the maximum G values, while the solid lines represent the minimum G values.

Table 4. Elastic anisotropy ratios of shear (G in GPa) and Young's (E in GPa) moduli of B_4N_4-I, B_4N_4-II, and c-BN.

Plane	Material	G_{max}	G_{min}	G_{max}/G_{min}	Plane	Materials	E_{max}	E_{min}	E_{max}/E_{min}
	B_4N_4-II	405.7	138.9	2.92		B_4N_4-II	899.4	382.2	2.35
(001)	B_4N_4-I	122.4	50.7	2.41	(001)	B_4N_4-I	556.2	94.2	5.90
	c-BN	433.0	314.0	1.38		c-BN	874.4	733.9	1.19
	B_4N_4-II	406.4	150.9	2.69		B_4N_4-II	862.6	377.7	2.28
(010)	B_4N_4-I	208.4	55.5	3.75	(010)	B_4N_4-I	704.2	74.3	9.48
	c-BN	433.0	314.0	1.38		c-BN	874.4	733.9	1.19
	B_4N_4-II	400.7	148.7	2.69		B_4N_4-II	865.5	555.7	1.56
(100)	B_4N_4-I	218.4	71.2	3.07	(100)	B_4N_4-I	556.2	74.3	7.49
	c-BN	433.0	314.0	1.38		c-BN	874.4	733.9	1.19
	B_4N_4-II	406.5	138.9	2.93		B_4N_4-II	930.6	350.6	2.65
All	B_4N_4-I	271.2	50.3	5.39	All	B_4N_4-I	704.2	74.3	9.48
	c-BN	433.0	314.0	1.38		c-BN	934.0	734.0	1.27

the maximal and minimal values of G for c-BN are the same in the primary planes, and they have the same shape in each plane. Moreover, G of c-BN exhibits the lowest mechanical anisotropy. In addition, the (001) plane of B_4N_4-II presents the highest mechanical anisotropy for G, while the (010) and (001) planes of B_4N_4-I present the highest and lowest mechanical anisotropies for G, respectively. The mechanical anisotropies of G for B_4N_4-II and B_4N_4-I in the three primary planes are all lower than those expressed for the materials as wholes (see Table 4). The 3D surface features of E for B_4N_4-II and B_4N_4-I are illustrated in Figs. 3(a) and 3(b), respectively. For isotropic systems, the 3D surface of E is spherical, and deviations from the spherical shape reflect the degree of elastic anisotropy for E.[56] From Figs. 3(a) and 3(b), B_4N_4-I may exhibit higher mechanical anisotropy for E. The 2D representations of E in the (001), (010), and (100) planes of B_4N_4-II and B_4N_4-I are illustrated in Figs. 3(c) and 3(d), respectively, and were used to analyze the anisotropies of B_4N_4-II and B_4N_4-I in detail.

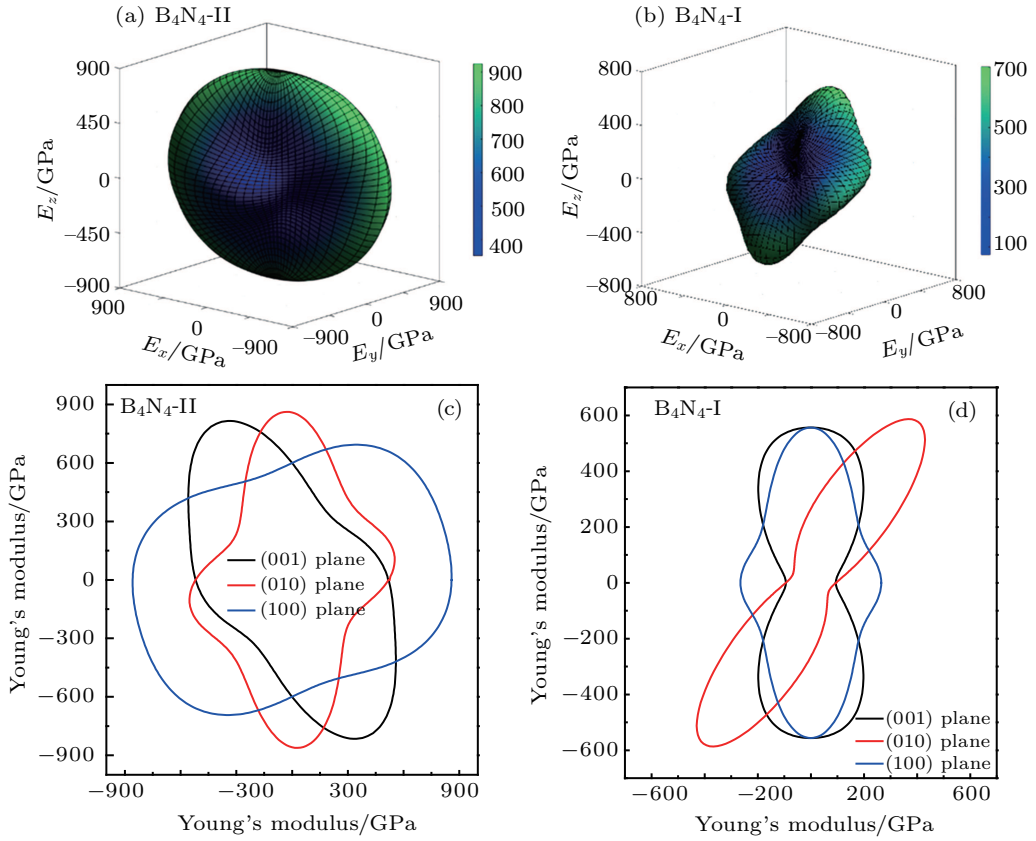


Fig. 3. Schematic 3D surface constructions of the Young's modulus E of (a) B_4N_4-II and (b) B_4N_4-I, and 2D representation of E of (c) B_4N_4-II and (d) B_4N_4-I. The black, red, and blue lines in panels (c) and (d) represent the (001), (010), and (100) planes, respectively.

The mechanical anisotropy of E in the (010) plane of B_4N_4-I is the highest. Similar to the method used to analyze G, we used the ratio of the maximum to minimum values of E to quantify the magnitude of elastic anisotropy. As can be seen, c-BN presented the same E_{max}/E_{min} ratio for the (010), (100), and (001) planes. Unsurprisingly, B_4N_4-I exhibited a much higher elastic anisotropy in the (001), (010), and (100) planes than B_4N_4-II. The mechanical anisotropies of E in the (001) and (100) primary planes of B_4N_4-II and B_4N_4-I were also lower than those expressed for the materials as wholes (see Table 4).

It is known that the band gap for the GGA–PBE functional is usually excessively underestimated, and therefore the experimental band gap should be greater than the calculated results (B_4N_4-II: 1.33 eV from the GGA–PBE functional[5] and 5.32 eV from the HSE06 hybrid functional). The results of many studies[2,57–63] support this conclusion. In the present study, the band structures of B_4N_4-II, B_4N_4-I, *Pbca*-BN, and c-BN were investigated using the HSE06 hybrid functional, and the results for B_4N_4-II and B_4N_4-I are illustrated in Figs. 4(a) and 4(b), respectively. From Fig. 4, the band gaps of B_4N_4-II and B_4N_4-I are indirect and wide, and their values are 5.32 eV and 4.86 eV, respectively. The Brillouin zones of B_4N_4-II and B_4N_4-I are depicted in Figs. 4(c) and 4(d), respectively. The valence band maximum and conduction band minimum of B_4N_4-II are located at the F and G points, while those of B_4N_4-I are located at the L and G points, respectively. The coordinates of the high-symmetry points in the Brillouin zone for B_4N_4-I are L $(-0.5,0.0,0.5)$, M $(-0.5,0.5,0.5)$, A $(-0.5,0.0,0.0)$, G $(0.0,0.0,0.0)$, Z $(0.0,-0.5,0.5)$, and V $(0.0,0.0,0.5)$; and those for B_4N_4-II are G $(0.0,0.0,0.0)$, Q $(0.0,0.5,0.5)$, Z $(0.0,0.0,0.5)$, and F $(0.0,0.5,0.0)$. The band

structures of *Pbca*-BN and c-BN are illustrated in Figs. 4(e) and 4(f), respectively. The band gap of *Pbca*-BN was 5.387 eV for the PBE functional, which was much closer to that reported by Fan *et al.*[6] (5.399 eV). The band-gap of *Pbca*-BN was 6.79 eV for the HSE06 hybrid functional, which was much greater than that of the PBE functional. The band gap of c-BN was 5.71 eV, which was close to the result of the HSE03 hybrid functional (5.99 eV).[64] The band gap of *Pnma*-BN was 7.18 eV[2] for the HSE06 hybrid functional, and was the largest among all BN polymorphs in this study. It is worth noting that *Pbca*-BN is a direct band gap material, while c-BN, *Pnma*-BN, B_4N_4-I, and B_4N_4-II are all indirect band gap materials.

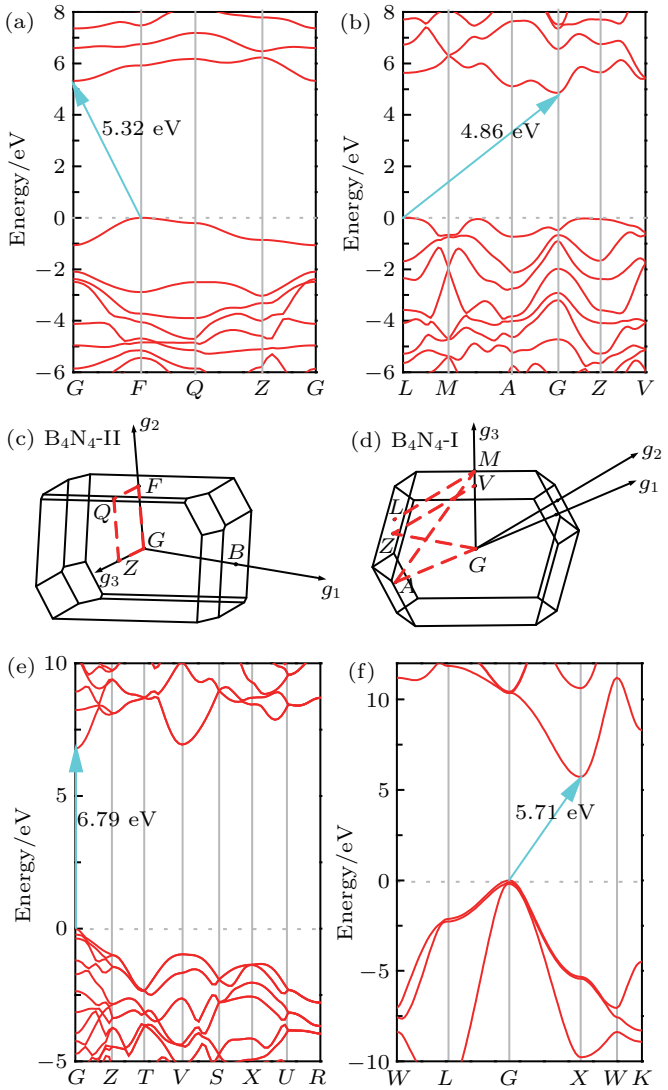


Fig. 4. Band structures of (a) B_4N_4-II and (b) B_4N_4-I. The dashed lines represent the Fermi level (E_F). Brillouin zones of (c) B_4N_4-II and (d) B_4N_4-I. Band structures of (e) *Pbca*-BN and (f) c-BN.

Thermal conductivity κ is one of the most important physical quantities that determines the efficiency of the semiconductors used in thermoelectric energy conversion processes. Cahill *et al.*[65] deduced the relationship between the minimum κ, κ_{min}, and temperature as follows:

$$\kappa_{min} = \left(\frac{\pi}{6}\right)^{1/3} k_B n^{2/3} \sum_i v_i \left(\frac{T}{\Theta_i}\right)^2 \int_0^{\Theta_i/T} \frac{x^3 e^x}{(e^x-1)^2} dx,$$

where the sum is obtained from the three sound wave velocities (two v_t and one v_l values), $\Theta_i = v_i[h/(2\pi k_B)](6\pi^2 n)^{1/3}$ is the cutoff frequency for each polarization, expressed in K, and n is the number density of atoms. This method of predicting κ has been applied in many studies.[42,66,67] The calculated κ_{min} values of B_4N_4-II, B_4N_4-I, and c-BN as a function of temperature are illustrated in Fig. 5. From Fig. 5, it can be seen that κ_{min} increases as the temperature increases. From 0 to 270 K, B_4N_4-I exhibits the highest κ_{min} of all three BN polymorphs illustrated in the figure; meanwhile, from 270 to 400 K, B_4N_4-II exhibits the highest κ_{min}. Furthermore, when the temperature is higher than 400 K, c-BN exhibits the highest κ_{min}. In addition, κ_{min} of B_4N_4-II at 300 K was 1.92 W/(cm·K), and it was slightly higher than that of B_4N_4-I and c-BN (1.84 W/(cm·K and 1.83 W/(cm·K, respectively). Moreover, κ_{min} of B_4N_4-I at 300 K was much closer to that of c-BN, but slightly higher than that of c-BN. As a wide band gap semiconductor material, c-BN presents high resistivity, high thermal conductivity, a low dielectric constant, a high breakdown electric field, high mobility, and double-type doping. Together with diamond, SiC, and GaN, which also exhibit wide band gaps, c-BN enables the use of electronic devices under extreme conditions. Moreover, c-BN and diamond feature other excellent properties, such as a wider band gap, higher breakdown electric field, higher mobility, lower dielectric constant, and higher thermal conductivity compared to SiC and GaN. Notably, as an extreme electronic material, c-BN is superior to diamond. The κ_{min} values of B_4N_4-II and B_4N_4-I were both slightly greater than that of c-BN, and therefore B_4N_4-II and B_4N_4-I may be more suitable than c-BN for electronic devices applications under extreme conditions.

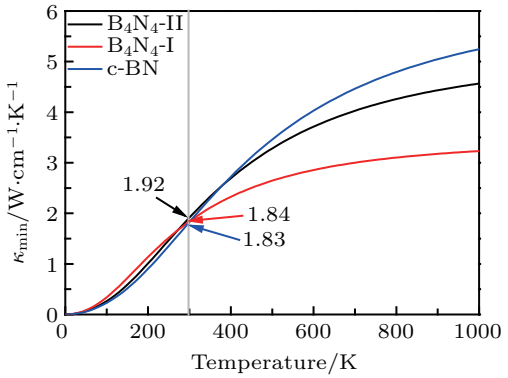


Fig. 5. Calculated minimum thermal conductivity (κ_{min}) of B_4N_4-I, B_4N_4-II, and c-BN as a function of temperature.

4. Conclusion

The structural, mechanical, electronic, and mechanical anisotropy properties, elastic anisotropies, and minimum ther-

mal conductivities of B_4N_4-I and B_4N_4-II were systemically investigated in the present study. The dynamical and mechanical stabilities of B_4N_4-I were demonstrated using phonon spectra and elastic constants, respectively, which revealed that B_4N_4-I was dynamically and mechanically stable. In addition, B_4N_4-I was brittle. The Debye temperatures of B_4N_4-II and B_4N_4-I were 1601 K and 1131 K, respectively. Anisotropy calculations indicated that the mechanical anisotropies of G and E of B_4N_4-II and B_4N_4-I were higher. The mechanical anisotropy of G in the (001) plane of B_4N_4-II was the highest of all three primary planes, while the elastic anisotropy of E in the (010) plane of B_4N_4-I was the highest of all three primary planes. Unsurprisingly, B_4N_4-I exhibited much higher E values in the (100), (010), and (001) planes than B_4N_4-II. Furthermore, B_4N_4-II and B_4N_4-I presented indirect and wide band gaps of 5.32 eV and 4.86 eV within HSE06 levels, respectively. At 300 K, the κ_{min} values of B_4N_4-II and B_4N_4-I were both slightly higher than that of c-BN.

Acknowledgment

The authors would like to thank Y. X. Song (School of Microelectronics, Xidian University) for allowing use of the Materials Studio CASTEP code.

References

[1] Wentorf R H 1957 *J. Chem. Phys.* **26** 956
[2] Ma Z Y, Han Z, Liu X H, Yu X H, Wang D Y and Tian Y 2016 *Nanomaterials* **7** 3
[3] Hromadová L and Martoňák R 2011 *Phys. Rev. B* **84** 224108
[4] Kuzubov A A, Tikhonova L V and Fedorov A S 2014 *Phys. Status Solidi B* **251** 1282
[5] Germaneau E, Su G and Zheng Q R 2013 *J. Phys.: Condens. Matter* **25** 125504
[6] Fan Q Y, Wei Q, Yan H Y, Zhang M G, Zhang Z X, Zhang J Q and Zhang D Y 2014 *Comput. Mater. Sci.* **85** 80
[7] Li Z P and Gao F M 2012 *Phys. Chem. Chem. Phys.* **14** 869
[8] Jiang X, Zhao J J and Ahuja R 2013 *J. Phys.: Condens. Matter* **25** 122204
[9] Dai J, Wu X J, Yang J L and Zeng X C 2014 *J. Phys. Chem. Lett.* **5** 393
[10] Doll K, Schön J C and Jansen M 2008 *Phys. Rev. B* **78** 144110
[11] Tang X, Hao J and Li Y W 2015 *Phys. Chem. Chem. Phys.* **17** 27821
[12] Reshak A H, Khan S A and Auluckc S 2014 *RSC Adv.* **4** 11967
[13] Wang X L 2012 *J. Chem. Phys.* **137** 184506
[14] Wang X L, Bao K, Tian F B, Meng X, Chen C B, Dong B W, Li D, Liu B B and Cui T 2010 *J. Chem. Phys.* **133** 044512
[15] Gong Y T, Li M M and Wang Y 2015 *ChemSusChem* **8** 931
[16] Fan Q Y, Chai C C, Wei Q and Yang Y T 2016 *Materials* **9** 427
[17] Mo S D, Ouyang L, Ching W Y, Tanaka I, Koyama Y and Riedel R 1999 *Phys. Rev. Lett.* **83** 5046
[18] Qiao L P and Jin Z 2017 *Materials* **10** 1413
[19] Zhang M G, Yan H Y, Zheng B B and Wei Q 2015 *Sci. Rep.* **5** 15481
[20] Li Y W, Li Q and Ma Y M 2011 *EPL* **95** 66006
[21] Zhou S and Zhao J J 2016 *Nanoscale* **8** 8910
[22] Wang S N, Oganov A R, Qian G R, Zhu Q, Dong H F, Dong X and Esfahani M M D 2016 *Phys. Chem. Chem. Phys.* **18** 1859
[23] Zhang X X, Wang Y C, Lv J, Zhu C Y, Li Q, Zhang M, Li Q and Ma Y M 2013 *J. Chem. Phys.* **138** 114101
[24] Sun H, Jhi S H, Roundy D, Cohen M L and Louie S G 2001 *Phys. Rev. B* **64** 094108
[25] Fan Q Y, Wei Q, Chai C C, Zhang M G, Yan H Y, Zhang Z X, Zhang J Q and Zhang D Y 2015 *Comput. Mater. Sci.* **97** 6
[26] Fan Q Y, Wei Q, Chai C C, Yan H Y, Zhang M G, Lin Z Z, Zhang Z X, Zhang J Q and Zhang D Y 2015 *J. Phys. Chem. Solids* **79** 89
[27] Krukau A V, Vydrov O A, Izmaylov A F and Scuseria G E 2006 *J. Chem. Phys.* **125** 224106
[28] Hohenberg P and Kohn W 1964 *Phys. Rev.* **136** B864
[29] Kohn W and Sham L J 1965 *Phys. Rev.* **140** A1133
[30] Vanderbilt D 1990 *Phys. Rev. B* **41** 7892R
[31] Pfrommer B G, Côté M, Louie S G and Cohen M L 1997 *J. Comput. Phys.* **131** 233
[32] Perdew J P, Burke K and Ernzerhof M 1996 *Phys. Rev. Lett.* **77** 3865
[33] Perdew J P and Zunger A 1981 *Phys. Rev. B* **23** 5048
[34] Monkhorst H J and Pack J D 1976 *Phys. Rev. B* **13** 5188
[35] Petrescu M I 2004 *Diamond Relat. Mater.* **13** 1848
[36] Li X Z and Xing M J 2018 *Comput. Mater. Sci.* **143** 32
[37] *Automatic – Flow for Materials Discovery*
[38] Wu Z J, Zhao E J, Xiang H P, Hao X F, Liu X J and Meng J 2007 *Phys. Rev. B* **76** 054115
[39] Xing M J, Li B H, Yu Z T and Chen Q 2015 *J. Mater. Sci.* **50** 7104
[40] Hill R 1952 *Proc. Phys. Soc. A* **65** 349
[41] Ma Z Y, Yan F, Wang S X, Jia Q Q, Yu X H and Shi C L 2017 *Chin. Phys. B* **26** 126105
[42] Fan Q Y, Chai C C, Wei Q, Zhou P K and Yang Y T 2017 *Mater. Design.* **132** 539
[43] Fan Q Y, Zhang W Z, Yun S N, Xu J and Song Y X 2018 *Chem. Eur. J.* **24** 17280
[44] Chen X Q, Niu H Y, Li D Z and Li Y Y 2011 *Intermetallics* **19** 1275
[45] Lyakhov A O and Oganov A R 2011 *Phys. Rev. B* **84** 092103
[46] Gao F M, He J L, Wu E D, Liu S M, Yu D L, Li D C, Zhang S Y and Tian Y J 2003 *Phys. Rev. Lett.* **91** 015502
[47] Xing M J, Li B H, Yu Z T and Chen Q 2016 *RSC Adv.* **6** 32740
[48] Bu H X, Zhao M W, Dong W Z, Lu S W and Wang X P 2014 *J. Mater. Chem. C* **2** 2751
[49] Bu H, Zhao M, Xi Y, Wang X, Peng H, Wang C and Liu X 2012 *Europhys. Lett.* **100** 56003
[50] Chen X Q, Niu H, Franchini C, Li D and Li Y 2011 *Phys. Rev. B* **84** 121405
[51] Pugh S F 1954 *Lond. Edinb. Dublin. Philos. Mag. J. Sci.* **45** 823
[52] Duan Y H, Sun Y, Peng M J and Zhou S G 2014 *J. Alloys Compd.* **595** 14
[53] Anderson O L 1963 *J. Phys. Chem. Solids.* **24** 909
[54] Panda K B and Ravi K S 2006 *Comput. Mater. Sci.* **35** 134
[55] Marmier A, Lethbridge Z A D, Walton R I, Smith C W, Parker S C and Evans K E 2010 *Comput. Phys. Commun.* **181** 2102
[56] Hu W C, Liu Y, Li D J, Zeng X Q and Xu C S 2014 *Comput. Mater. Sci.* **83** 27
[57] Sun M L, Chou J, Gao J F, Cheng Y, Hu A, Tang W C and Zhang G 2018 *ACS Omega* **3** 8514
[58] Sun M L, Ren Q Q, Wang S K, Yu J and Tang W C 2016 *J. Phys. D* **49** 445305
[59] Fan Q Y, Chai C C, Wei Q, Zhou P K, Zhang J Q and Yang Y T 2016 *Materials* **9** 284
[60] Sun M L, Chou J, Shi L H, Gao J F, Hu A, Tang W C and Zhang G 2018 *ACS Omega* **3** 5971
[61] Tang W C, Sun M L, Ren Q Q, Zhang Y J, Wang S K and Yu J 2016 *RSC Adv.* **6** 95846
[62] Xu X Y, Chai C C, Fan Q Y and Yang Y T 2017 *Chin. Phys. B* **26** 046101
[63] Sun M L, Chou J, Zhao Y M, Yu J and Tang W C 2017 *Phys. Chem. Chem. Phys.* **19** 28127
[64] Heyd J, Peralta J E, Scuseria G E and Martin R L 2005 *J. Chem. Phys.* **123** 174101
[65] Cahill D G, Watson S K and Pohl R O 1992 *Phys. Rev. B* **46** 6131
[66] Fan Q Y, Niu R, Zhang W Z, Zhang W, Ding Y C and Yun S N 2019 *ChemPhysChem* **20** 128
[67] Fan Q Y, Chai C C, Wei Q, Wong K Q, Liu Y Q and Yang Y T 2018 *J. Mater. Sci.* **53** 2785